INTRODUCTION

Cancer is currently one of the leading causes of death, with roughly 9.6 million deaths annually globally and about 18.1 million newly diagnosed cancer cases every year (Bray et al., 2018). One of the most lethal types, as well as one of the most common types, is pancreatic ductal adenocarcinoma (PDAC) (Xialiang et al., 2018). PDAC is an exocrine cancer (Smigiel et al., 2018) that is derived from the ducts of the pancreas (Ferreira et al., 2017) and makes up roughly 90% of all pancreatic cancers (Xialiang et al., 2018), making it the 12th most common cancer worldwide (Hall et al., 2018). Unfortunately, PDAC only has a 9% 5-year survival rate (Kenner et al., 2017), with pancreatic cancer as a whole constituting 7% of all cancer deaths (M. Ilic & I Ilic, 2016), making it the 4th deadliest cancer in the United States, (Pelosi et al., 2017); by 2020, it is expected to be the 2nd deadliest (Garrido-Laguna et al., 2015).

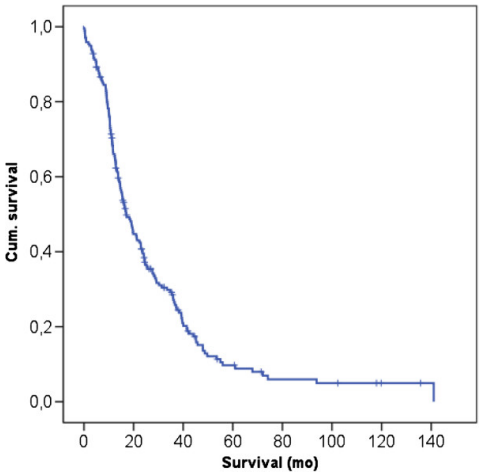

Figure 1: Graph of survival rate of PDAC patients over time (Distler et al., 2013) - 1.0 on the y-axis signals 100% survival rate, and 0.0 on the y-axis signals 0% survival rate. By 140 months, survival rate is about 5%.

Unfortunately, due to the current lack of reliable therapeutic options for PDAC in-clinic, tumor resection surgery is the best method to treat this cancer (Kuang & Xu Tian Lao, 2015). Furthermore, since the pancreas is located near many major blood vessels (Buchs et al., 2010), and PDAC is a hyper-aggressive cancer that typically asymptomatic until metastasizing has begun (Deshwar et al., 2018), opportunities for tumor resection surgery is rare. Only about 15-20% PDAC patients can undergo tumor resection surgery upon diagnosis (Deshwar et al., 2018). At the root of this low survival rate is indubitably the consistent failure to diagnose PDAC at

earlier stages, as well as the frequent misdiagnosis of PDAC. Approximately 31.3% of people with PDAC are misdiagnosed with other types of cancers, often resulting in unnecessary surgeries/treatment before the mistake is realized (Swords et al., 2015). Obviously, the asymptomatic characteristics of PDAC also play a role in these consistent late diagnosis of PDAC, but unavailability of reliable treatments and efficient techniques to diagnose PDAC is also worth recognition.

Currently, a Positron Emission Tomography (PET) scan following the injection of the "golden standard" 2-deoxy-2-[fluorine-18]fluoro-D-glucose (^{18}F-FDG) PET tracer poses the most dependable method of PDAC detection (Yasuda et al., 2000).

^{18}F-FDG exhibits a 86.7% detection rate for PDAC and has only about an average 54% detection rate for all cancers (Yasuda et al., 2000), however,^{18}F-FDG is readily taken up by both healthy and cancerous cells (Aruna et al., 2015). The radiation emitted by the radioactive ^{18}F in ^{18}F-FDG can damage healthy cells, leading to cell death or, worse, new cancer growth elsewhere in the body (Little, 1970). Thus a new method of detecting and imaging PDAC is needed.

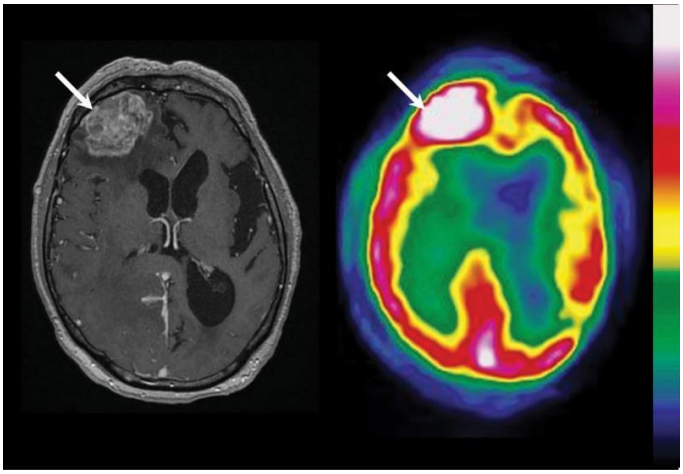

Figure 2: Depiction of an ^{18}F-FDG PET scan (Verger, 2017). Although the tumor in this situation, shown by the arrow, is clearly outlined, with the majority of the ^{18}F-FDG accumulating there, a large amount also accumulates elsewhere in the brain, putting the patient at risk of cell death, developing cancers due to DNA mutation from radiation, and more.

Currently, there are two major ways of using PET-based tracers to detect malignant tissue: through the use of synthesized nanopolymers or through the use of antibodies

(Torchilin, 2010). The methods by which the nanopolymers reach their target tumor locations have been separated into two subcategories: active targeting and passive targeting (Torchilin, 2010), whereas antibodies primarily reach their target location through the highly-specific use of antigens, to which only that specific antibody can bind to (Attarwala, 2010)

Active targeting encompasses any method by which nanopolymers reach their target tumor through receptor-ligand interactions (Biswajit et al., 2013). This allows for the binding of certain ligands located on these nanopolymers to specific receptors often located on the surface membranes of cancerous cells, hence binding the nanopolymers to the surface membranes of these cells (Biswajit et al., 2013). Tumors can be imaged through the imaging of the radioisotopes attached to these nanopolymers through various methods.

Passive targeting of nanopolymers utilizes the Enhanced Permeability and Retention (EPR) effect for nonspecific imaging of the cancerous tumors (Ljubimova & Eggehard, 2012). The EPR effect is a phenomenon of leaky vasculature and an impaired lymphatic drainage system caused by the need of tumor cells to receive their necessary oxygen and nutrients (Greish, 2010). When tumors grow larger, the delivery of oxygen and nutrients become more limited. To increase resources availability, a developing tumor will begin to release angiogenic factors, such as bradykinin and nitric oxide, resulting in increased angiogenesis (Bazak et al., 2014). As the tumor grows in size, the amount of such factors that it releases continues to increase. Consequently, the continued angiogenesis results in disorganized, dilated blood vessels with many pores and gaps between their endothelial cells (Bazak et al., 2014). Nanopolymers can then slip through the endothelial cells, falling into the tumor microenvironment, and can be effectively imaged from there, allowing for imaging of the tumor as well (Bazak et al., 2014).

The other primary method of imaging tumors with PET tracers is through the use of antibodies. This specific method of imaging works similarly to active targeting with nanopolymers, in that the antibodies are first chelated and then radiolabeled. These labeled antibodies can detect tumors by interacting with specific molecules in the tumor microenvironment; in this case, those molecules are certain antigens typically created exclusively by those tumor cells (Goldenberg, 1993).

Previous studies attempting to delineate PDAC tumors through the use of antibody-antigen interactions have focused on the interaction between the monoclonal antibody (5B1) and the antigen Carbohydrate Antigen 19.9, or CA19.9 (Viola-Villegas et al., 2013). However, CA19.9 is an antigen not exclusive to pancreatic cancers (Poruk et al., 2013), or PDAC. CA19.9 it was first discovered to be expressed by colorectal carcinoma cells (Poruk et al., 2013) and since shown to be expressed in other cancerous and non-cancerous conditions (Safi et al., 1989). Concerning antibody uptake, numerous studies have shown using PET scans that PDAC tumor can significantly take up the radiolabeled 5B1 (Houghton et al., 2017). However, since CA19.9 is rarely present in asymptomatic populations (Poruk et al., 2013), it is difficult to use this antigen-antibody interaction as suboptimal imaging agent for early diagnosis of PDAC. CA19.9

is also often shed into circulation rather than remaining on surface membranes of cells (Haglund et al.,1989), resulting in relatively high radiation exposure to other parts of the body.

There have also been other relatively successful studies for imaging PDAC tumors that utilize the Carcinoembryonic Antigen (CEA) biomarker, however, similarly to CA19.9, it is typically not expressed by asymptomatic populations ("Cancer Markers", 2013), and is also shed into circulation (Abdul-Wahid et al., 2018).

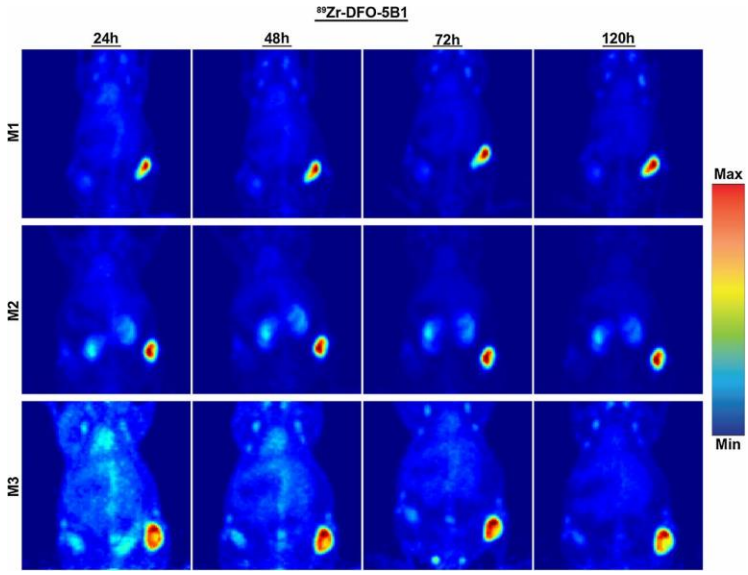

Figure 3: PET scans using a radiolabeled 5B1 antibody (Houghton et al., 2015) - the corresponding antibody to CA19.9. The images are much more clear than, for example, those of an ^{18}F-FDG PET scan, and using 5B1 seems to be an efficient way of detecting PDAC tumors, but there is also, as seen in all images, noticeable radiation exposure to healthy cells, likely due to the cell being shed into circulation.

Since there is no reliable antigenic markers, it is important to identify new antigenic markers that are exclusive to PDAC and are not shed into circulation as the cancer progresses. One method that is explored to identify antigens specific to PDAC is through the development of organoids.

Organoids are complex organ-like structures model systems that can be grown and analyzed in-vitro (Holloway et al., 2019). They are frequently derived from human pluripotent stem cells or primary human

donor tissue (Holloway et al., 2019) and are capable of differentiating into various different types of cells (Xu et al., 2018).

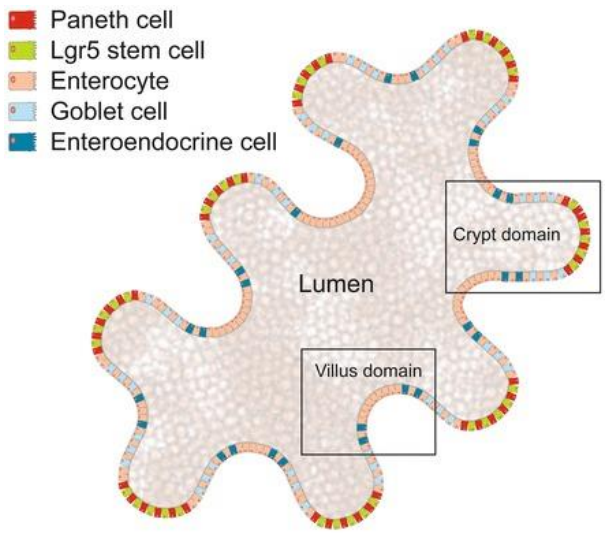

Figure 4: Digital example of an intestinal organoid (Lukovac, 1970). Unlike growing simply epithelial cells, growing an organoid will yield a wider range of cell types, making it ideal for modeling certain organs. Several different types of intestinal cells are present here, including enterocytes and enteroendocrine cells, and the organoid even grew villus and crypt domains as well as lumen. This organoid was grown from Lgr5 intestinal stem cells (Lukovac, 1970)

The fact that organoids can be differentiated into many different type of complex cells, making them like mini organs, combined with the fact that organoids can be studied and grown in-vitro makes them incredibly reliable for experimentation (Xu et al., 2018). Organoids can be used to obtain antibodies for antigens that are of interest, such as antigens located on surface membranes of PDAC cells. For this, the organoids would have to be crushed together, and then their cell surface membrane fragments isolated (Unpublished research). The membrane fragments would be injected into the animal of choice, which would create antibodies to the antigens on the surface membranes (Unpublished research). From here, the most efficient method of obtaining the respective antibodies to all of the antigens on the PDAC cell surface membranes and then cloning them (hence the name, monoclonal antibodies) would be by harvesting the spleens of the animals, and then creating hybridomas (Unpublished research). In the body, the cells responsible for creating antibodies are lymphocyte B cells, which are located in the spleen; to create a hybridoma, B cells are fused with cancerous myeloma cells,

which will then proceed to multiply indefinitely, creating cancer cells that are capable of producing the desired monoclonal antibodies (Mukherjee et al., 2013). Since any animal with a functioning immune system will have large amounts of different types of B cells producing different types of antibodies at any given time (Unpublished research), this method of monoclonal antibody production will yield large amounts of antibodies, many of which may not even correspond to antigens related to the target cancer (Unpublished research). Through various sorts of tests, such as immunohistochemical staining, the antibodies exclusive to antigens in the target cancer can be isolated (Unpublished research).

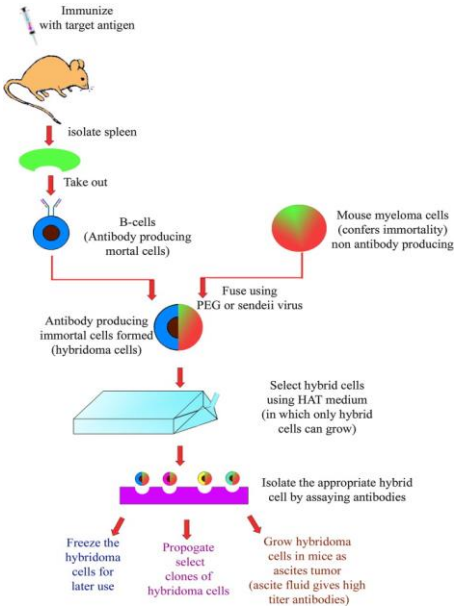

Figure 5: Representation of how to create a hybridoma for a particular monoclonal antibody (Khan, 2013) - begin by isolating the spleen, then take out the B-cells, and fuse that with a myeloma cell. From there, the hybridoma cells are selected using a hypoxanthine-aminopterin-thymidine (HAT) medium in which only hybrid cells can grow. From there, appropriate hybrid cells for particular monoclonal antibodies can be isolated by assaying the antibodies.

Through such a process, two antibodies - AB1 and AB2 - were successfully isolated (Unpublished research). This showed that antibodies AB1 and AB2 bind to an antigen that is exclusively found in malignant tissue, including PDAC tissue, however, the antibody had yet to be radiolabeled and then used to detect PDAC tumors (Unpublished research). This study investigates if the antibodies can successfully reach a PDAC tumor - other factors, such as the antibody's stability in-vivo and the stability of the antigen to the malignant cells' membranes.

METHODOLOGY

All handling of radioactively-labelled antibodies, tissue, and animal studies were performed by mentor. I solely analyzed the results from these experiments.

For data analysis, Microsoft Excel, the BIOSCAN AR 2000, imageJ, the 3D Slicer software (v4.8.1), and the Inveon Research Workspace software (Siemens Medical Solutions, Knoxville, USA) were used.

The BIOSCAN AR 2000 was used to construct graphs of radiochemical purity after performing the iTLCs, and then to more accurately determine the exact radiochemical yields.

After PET scans were performed, individual image volumes were constructed using the cropping function of the Inveon Research Workspace software. To determine the actual activity concentrations, in Percent Injected Dose per gram (% ID/g), of the images, the counting rates were converted using a system calibration factor, which was derived from a mouse-sized water-equivalent phantom containing ^{89}Zr. To finish constructing the images, the 3D Slicer software was used.

The weights of each tissue were then calculated, and the radioactivity bound to each tissue, measured in % ID/g, was calculated using the 2480 Wizard gamma counter (performed by mentor). Excel was then used to calculate the percentage of tracer uptake in each certain specific tissue samples, expressed as % ID/g, as the activity bound to the tissue per tissue weight per the actual injected dose, decay-corrected to the time of counting. Relevant graphs and charts composed of the calculated data were then constructed.

ImageJ was used on the immunohistochemical stainings to quantify the percentage of stained tissue area versus the percentage of unstained tissue area. The higher the percentage of

stained area in the stainings, the higher the presence of an antigen being targeted by the subject antibody in that specific tissue type.

RESULTS:

Immunohistochemical Staining Analysis

From the organoids, various monoclonal antibodies were developed that recognized specific surface antigens. Of these antibodies, two showed very more specific recognition of PDAC. These antibodies were designated AB1 and AB2. Analysis of immunohistochemically-stained PDAC and other malignant tissue showed that AB1 has a designated affinity for various different malignancies, not just PDAC, including invasive ductal adenocarcinoma of the breast, medullary carcinoma of the breast, squamous cell carcinoma of the uterine/cervix, serous adenocarcinoma of the ovaries, transitional cell carcinoma of the bladder, colorectal carcinoma, hepatocellular carcinoma, bronchioalveolar carcinoma, and stomach adenocarcinoma. Further analysis of the immunohistochemically stained tissue showed that AB2 has a designated affinity for other malignancies as well, including invasive ductal carcinoma of the breast, rectal adenocarcinoma, colorectal carcinoma, hepatocellular carcinoma, bronchioalveolar carcinoma, and stomach adenocarcinoma.

Analysis showed that, for the most part, neither of the two antibodies bind to any normal tissue, which included healthy pancreatic tissue, colon tissue, and stomach tissue. AB1 did seem to bind minimally to tissue from the salivary glands, however, and this was reflected in the PET scans. This means that the antigen that the antibodies bind to is exclusively produced by malignant cancer cells, and not by normal tissue.

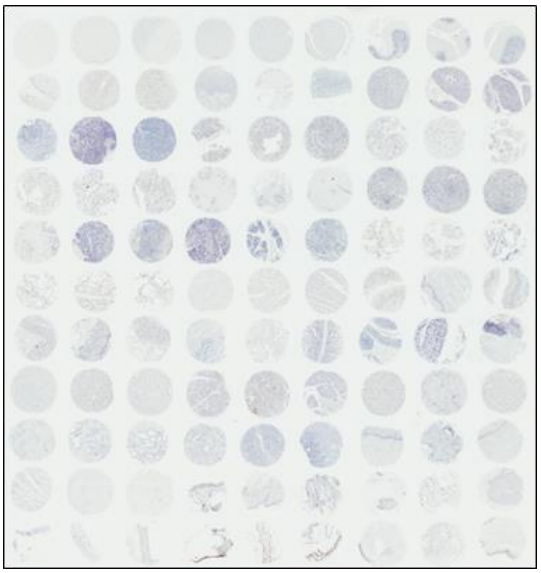

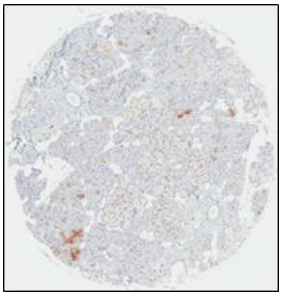

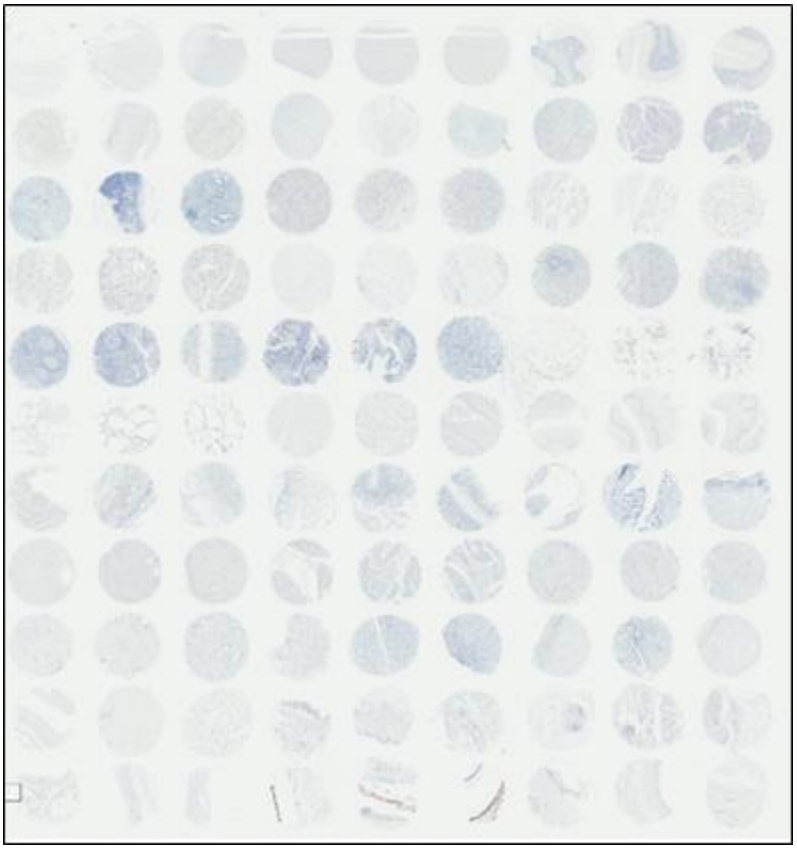

Figure 6 & Table 1: Immunohistochemical stainings of antibodies AB1 and AB2, respectively, as they bind to normal, healthy tissue. As seen in the table, AB1 appears to bind to antigens in the salivary glands to a certain extent, but does not bind to any other healthy tissue. AB2 does not bind to any antigens in the healthy tissue. The secondary picture next to the image of AB1 is a close-up of the positive immunohistochemically stained salivary glands by AB1.

Tissue	% Binding AB1	% Binding AB2
Salivary glands	9.8	0
Stomach	0	0
Liver	0	0
Lung	0	0

Analysis upon the immunohistochemical stainings to identify the rough percentage of each sample to which the antibodies bind to was performed using ImageJ - the higher the percentage, the higher the presence of the antigen in that specific tissue sample, and hence, the higher the viability of the use of some sort of radiotracer based on this antibody in the future. For AB1, 9.8% binding was found in salivary glands, with 0% for any other type of healthy tissue.

Meanwhile, it exhibited 57.1% binding to PDAC tissue, 71.3% binding to breast invasive ductal carcinoma tissue, 96.1% to breast medullary carcinoma tissue, 43.4% to squamous cell carcinoma of the uterine, 49.5% to serous adenocarcinoma of the ovaries, 59.7% to transitional cell carcinoma of the bladder, 91.9% to colorectal carcinoma, 41.1% to hepatocellular carcinoma, 61.9% to bronchioalveolar carcinoma, and 45.5% to stomach adenocarcinoma. for AB2, no binding was recorded for any type of healthy tissue, but it did exhibit high percents of binding with the malignant tissues.

AB2 exhibited 50.2% binding to PDAC, 69.9% binding to invasive ductal carcinoma of the breast, 97.7% binding to medullary carcinoma of the breast, 46.8% binding to squamous cell carcinoma of the uterine, 50.7% binding to serous adenocarcinoma of the ovaries, 52.3% binding to transitional cell carcinoma of the bladder, 94.3% binding to colorectal carcinoma, 57.6% binding to hepatocellular carcinoma, 39.6% binding to bronchioalveolar carcinoma, and 51.3% binding to stomach adenocarcinoma. It is worth mentioning that rat IgG was used as a control for the normal tissue, exhibiting minimal to no binding to most tissue, but also binding with 41.3% to the eyes, 67.9% to the stomach, and 19.8% to the colon. It also did not show any binding to PDAC tumor tissue, normal pancreatic tissue, or pancreatic tissue adjacent to the tumor. In this,

AB1 showed a similar pattern to AB2 in terms of what it bind to and the percentage of each tissue sample that it binded to.

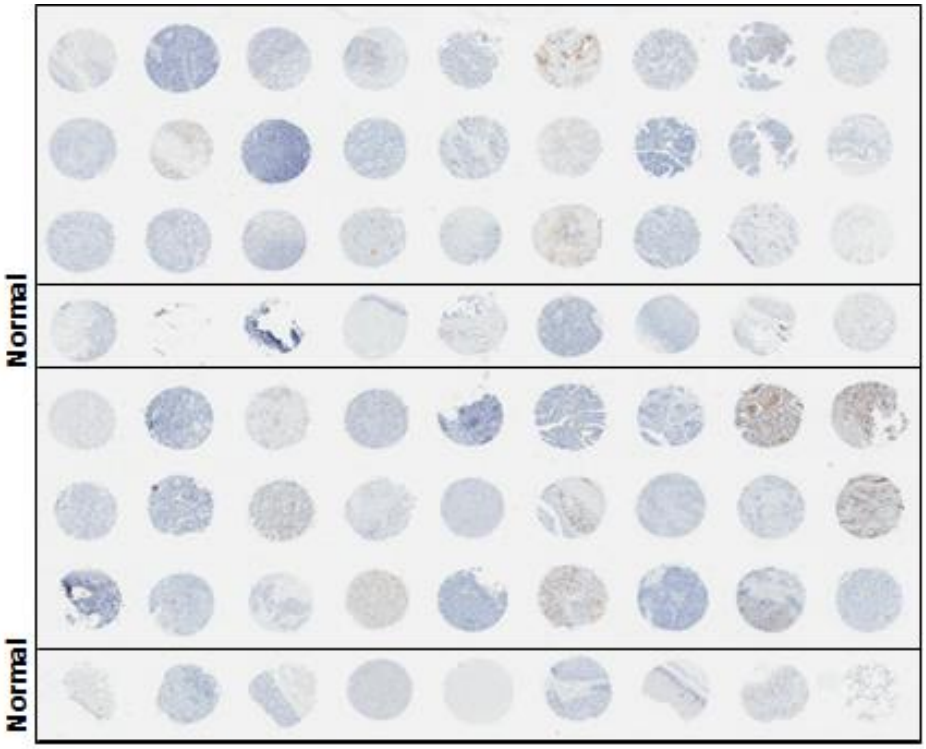

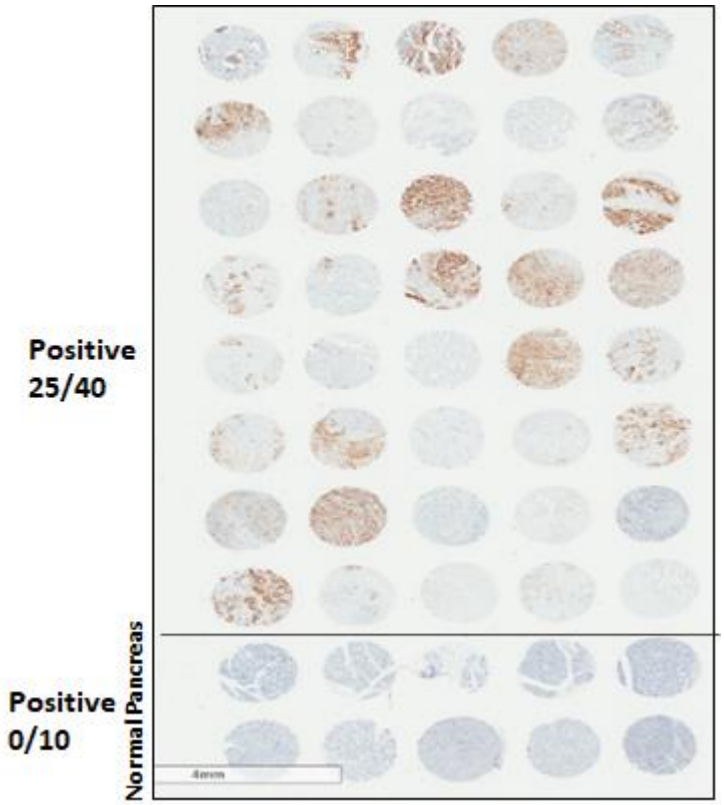

Tissue	% Binding AB1
PDAC	57.1
Transitional cell carcinoma of the bladder	59.7
Bronchioalveolar carcinoma	61.9
Squamous cell carcinoma of the uterine	43.4
Serous adenocarcinoma of the ovaries	49.5
Breast invasive ductal carcinoma	71.3
Hepatocellular carcinoma	41.1
Breast medullary carcinoma	96.1
Colorectal carcinoma	91.9
Stomach adenocarcinoma	45.5

Figure 7 & Table 2: Immunohistochemical stainings of AB1, for the top figure, with varying malignant tissue samples, and for the bottom, with PDAC tissue samples and healthy pancreatic tissue samples. The top figure indicates that AB2 binds to an antigen in several malignant tissues, including stomach adenocarcinoma, colorectal carcinoma, and bronchioalveolar carcinoma; this is further supported by the data shown in the table. A comparison for the normal tissue samples that the malignant tissues are derived from (i.e., healthy stomach tissue with stomach adenocarcinoma tissue) is shown beneath the tissue samples in the top figure). The second figure shows that AB1 does not bind to healthy pancreatic tissue, while still binding to PDAC tissue, binding 0/10 cases to healthy pancreatic tissue, and 25/40 cases to PDAC tissue.

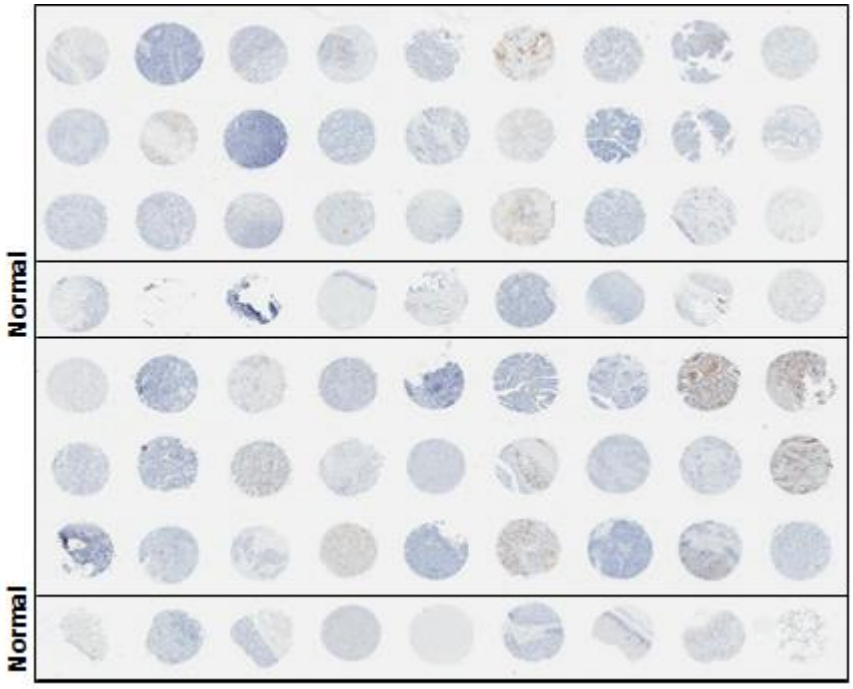

Tissue	% Binding AB1
PDAC	50.2
Transitional cell carcinoma of the bladder	52.3

Bronchioalveolar carcinoma	39.6
Squamous cell carcinoma of the uterine	46.8
Serous adenocarcinoma of the ovaries	50.7
Breast invasive ductal carcinoma	69.9
Hepatocellular carcinoma	57.6
Breast medullary carcinoma	97.7
Colorectal carcinoma	94.3
Stomach adenocarcinoma	51.3

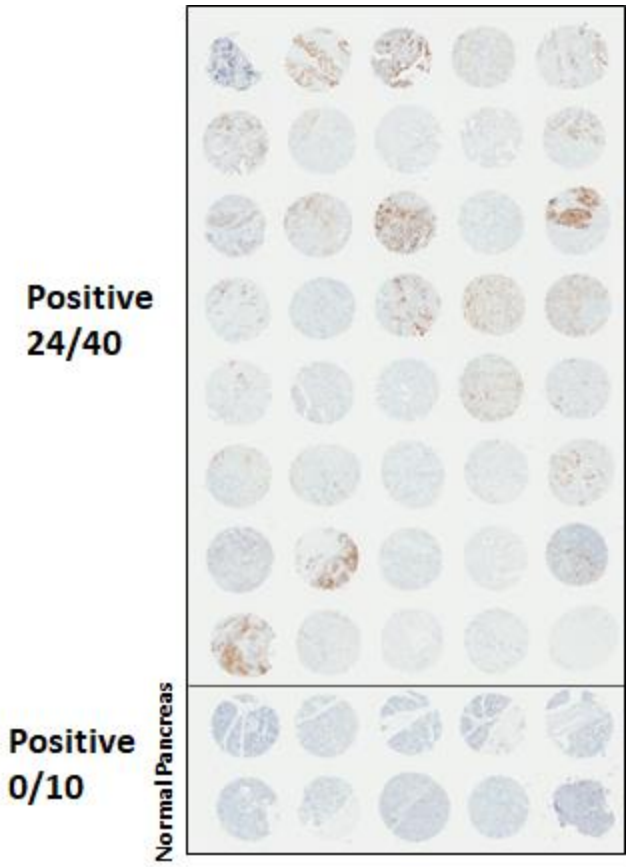

Figure 8 & Table 3: Immunohistochemical stainings of AB2, for the top figure, with varying malignant tissue samples, and for the bottom, with PDAC tissue samples and healthy pancreatic tissue samples. The top figure indicates that AB2 binds to an antigen in several malignant tissues, including stomach adenocarcinoma, colorectal carcinoma, and hepatocellular carcinoma; this is further supported by the data shown in the table. A comparison for the normal tissue samples that the malignant tissues are derived from (i.e., healthy stomach tissue with stomach adenocarcinoma tissue) is shown beneath the tissue samples in the top figure). The second figure shows that AB2 does not bind to healthy pancreatic tissue, while still binding to PDAC tissue, binding 0/10 times to healthy pancreatic tissue, and 24/40 times to PDAC tissue.

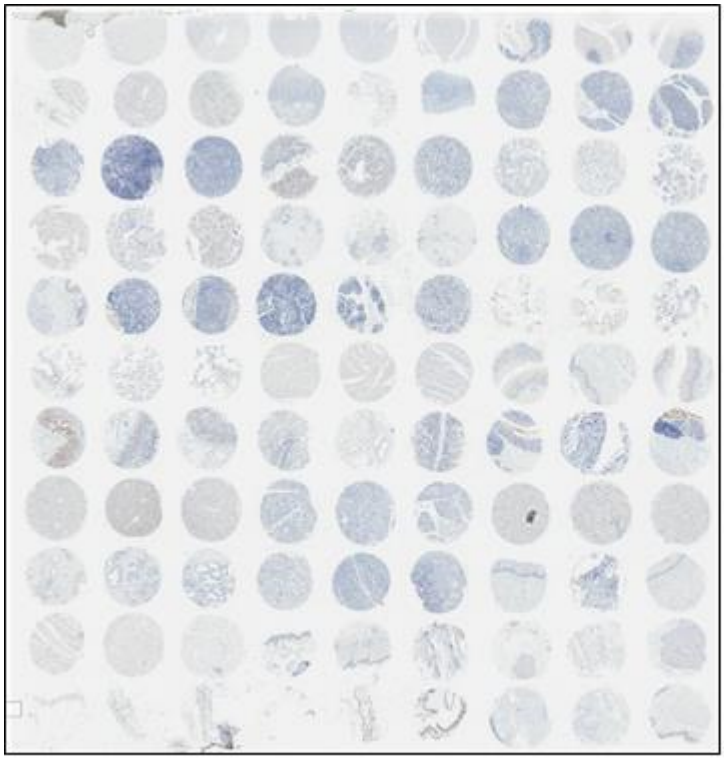


Stomach

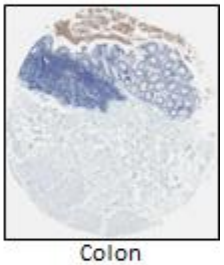
Colon


Eyes

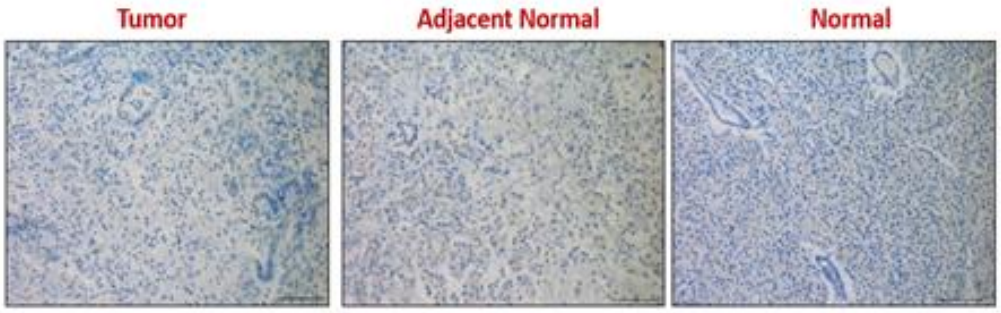

Tissue	% Binding IgG
Eyes	41.3
Stomach	67.9
Colon	19.8
Salivary glands	0

Figure 9 & Table 4: Immunohistochemical stainings of rat IgG. The top figure shows IgG immunohistochemical stainings to normal, healthy tissue, whereas the bottom figure shows IgG staining to the normal, healthy pancreas, PDAC tissue, and healthy pancreatic tissue adjacent to the PDAC tissue. IgG did not bind at all to the PDAC, pancreatic tissue adjacent to the PDAC, or normal, healthy pancreatic tissue, but it did bind to certain healthy tissues, including at 19.8% binding to colon tissue, 41.3% binding to the eyes, and 67.9% binding to the stomach. It did not bind to all tissue, however, such as to the salivary glands, as AB1 did.

Stability Assays

To confirm the stability of antibodies AB1 and AB2 in-vivo, a stability assay was performed. The antibodies were suspended in saline solution and phosphate-buffered saline (PBS) solution as controls, and then in human serum, at 37°C for 24 hours. As seen in Figure 10,

the antibodies remained completely intact in all cases except, for AB2, in the saline solution; roughly **7%** of the antibodies seemed to break down. In all other situations, the antibodies remained 100% intact, indicating that the antibodies will remain intact in humans and mice.

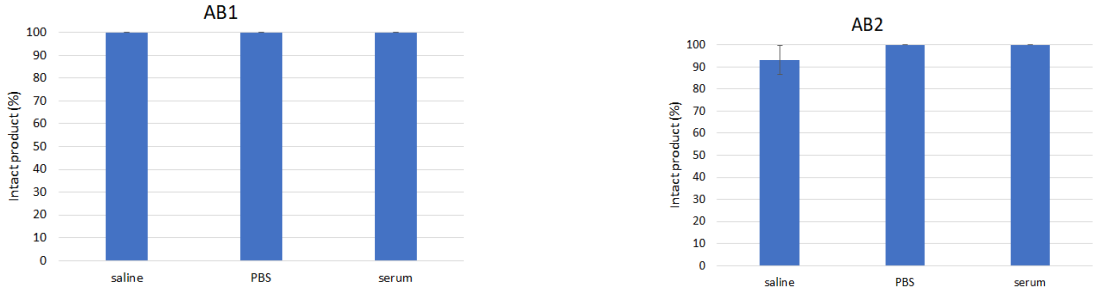

Figure 10: Stability assays of AB1 and AB2. AB1 and AB2 were exposed to saline, PBS, and human serum solutions, and left in them in 37°C for 24 hours. AB1 and AB2 stayed 100% intact in all conditions except for AB2 in saline, but they both remained fully stable in serum.

Radiolabeling of ^{89}Zr to AB1 and AB2

Mentor radiolabeled ^{89}Zr to AB1 and AB2, and efficacy of radiolabeling was determined through use of an iTLC. Radiochemical yield and radiochemical purity were both determined to be >99 for both antibodies, seen in Figure 11 and Table 5, indicating successful radiolabeling.

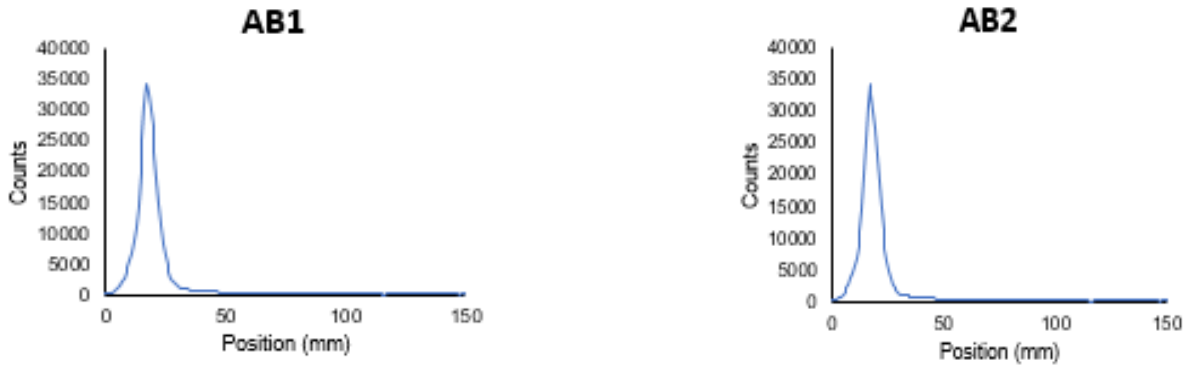

Figure 11: iTLC analyses. One maximum indicates the presence of only one radiolabeled compound. The compound in this case is the respective radiolabeled antibody

	AB1	AB2
Radiochemical yield (%)	>99	>99
Radiochemical purity (%)	>99	>99
Specific activity (μCi/μg)	16.7	14.3

Table 5: iTLC indicates that the ^{89}Z was radiolabeled to both antibodies successfully. >99% radiochemical purity for both radiolabeled antibodies signifies that >99% of the antibodies in the given samples were successfully radiolabeled, and >99% radiochemical yield in both antibodies indicates that >99% of the original radioactivity before the radiolabeling was retained in the radiolabeled antibodies. Specific activity given by the iTLC indicates sufficient radioactivity to perform the ensuing experiment.

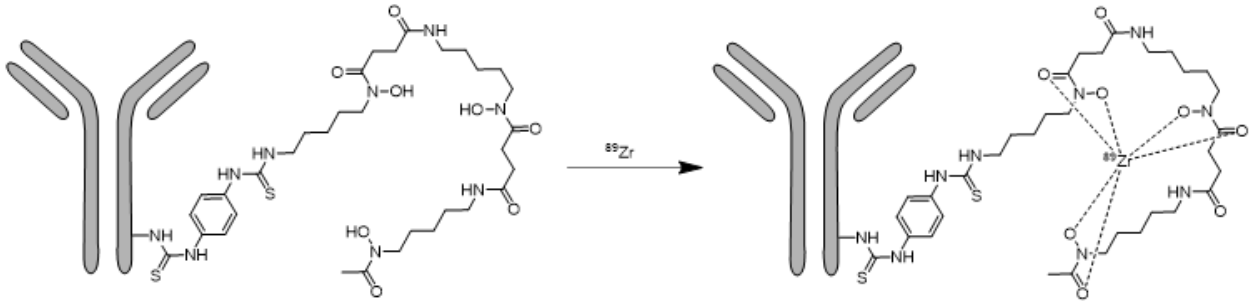

Figure 12: Visual diagram of desferrioxamine (DFO)-chelated sample antibody. The DFO chelator serves to allow the ^{89}Zr, a metal, to bind to the antibody.

[^{89}Zr]Zr-DFO-AB1 and [^{89}Zr]Zr-DFO-AB2 bind to PDAC tumors

PET imaging shows specific accumulation and retention of [^{89}Zr]Zr-DFO-AB1 and [^{89}Zr]Zr-DFO-AB2 in Suit-2 tumorbearing mice, particularly over 24 to 144 hours post-injection, signalled by high % ID/g of the radiolabeled antibodies in the mice in 1 day, 3 day, and 6 day timepoints, seen in Figure 13. Biodistribution data of the antibodies in varying organs and tissue of the mice indicated similar results, seen in Figures 14a and 14b, with high % ID/g of AB1 and AB2 in the PDAC tumors and minimally elsewhere following the 1 day timepoint; prior to 1 day, high accumulation in the blood, lungs, and heart could also be seen. Accumulation in liver and kidneys was also relatively high throughout each timepoint.

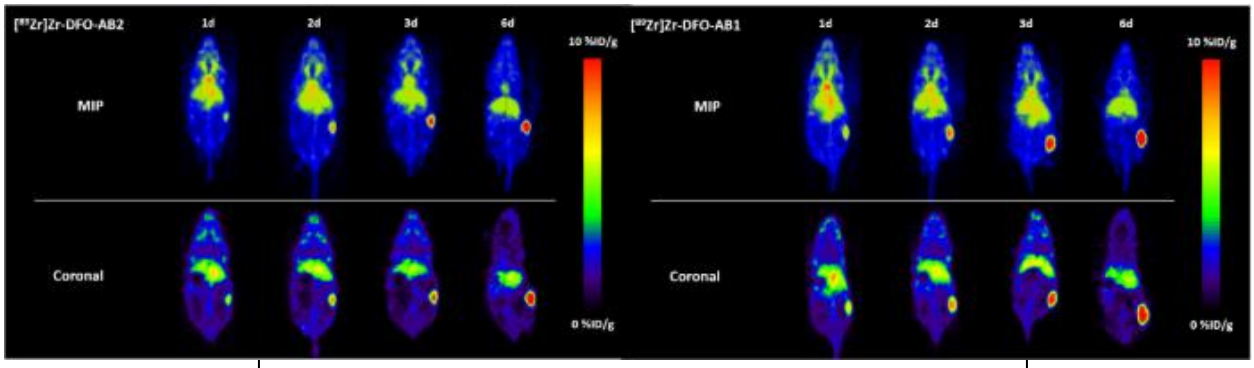

Figure 13: PET images depicting mice 1 day, 2 days, 3 days, and 6 days post-injection. PET images were not taken prior to the 1 day time point because they would likely not have accumulated well in the tumor yet, and would likely only show high uptake in blood. High % ID/g is seen in the tumors of the mice, shown by a redder color, especially in the later time points, indicated high accumulation and retention of radiolabeled AB1 and AB2 in the tumors

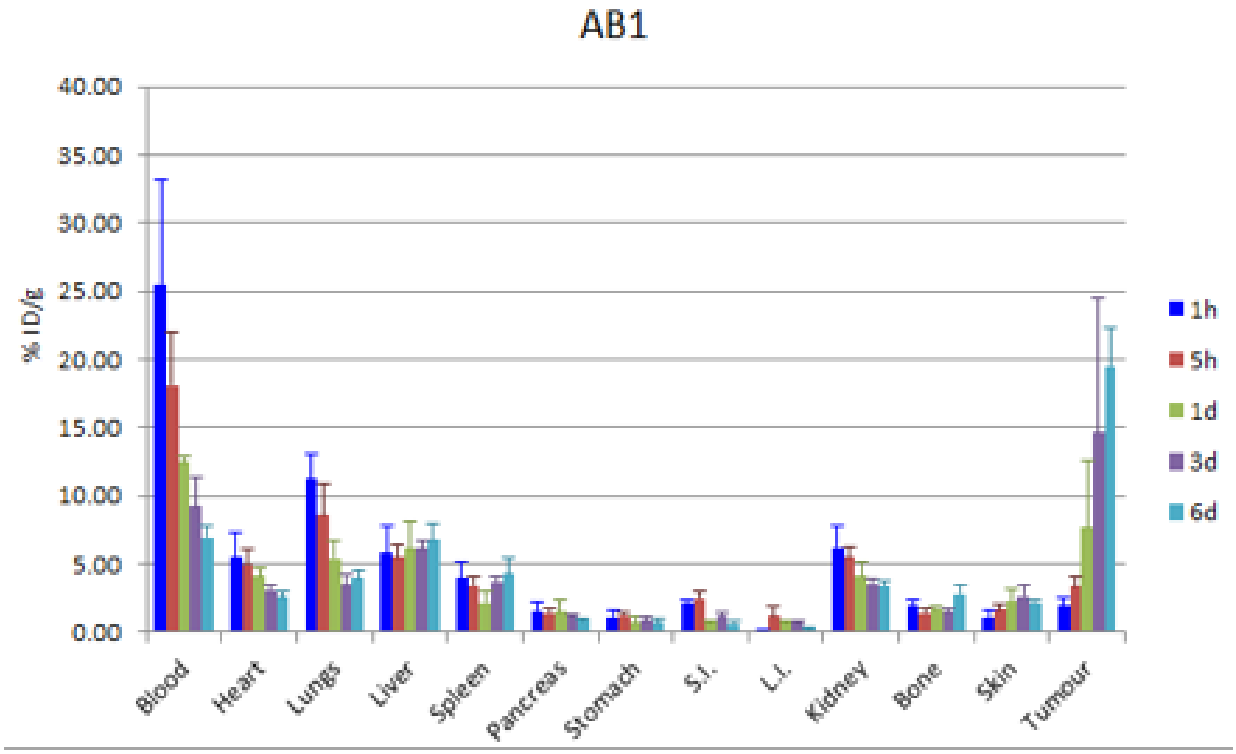
AB1
40.00
35.00
30.00
25.00
20.00
15.00
10.00
5.00
0.00
% ID/g
Blood
Heart
Lungs
Liver
Spleen
Pancreas
Stomach
S.I.
L.I.
Kidney
Bone
Skin
Tumour
1h
5h
1d
3d
6d

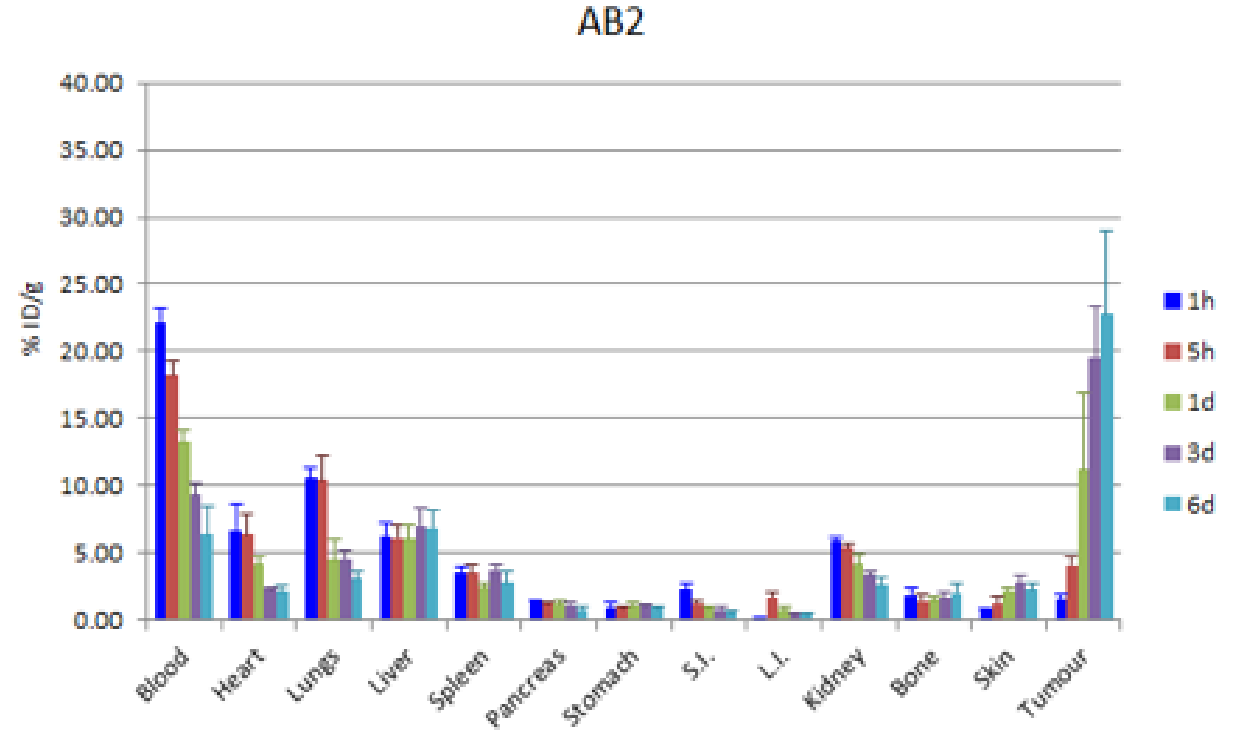
AB2
40.00
35.00
30.00
25.00
20.00
15.00
10.00
5.00
0.00
% ID/g
Blood
Heart
Lungs
Liver
Spleen
Pancreas
Stomach
S.I.
L.I.
Kidney
Bone
Skin
Tumour
1h
5h
1d
3d
6d

Figures 14a and 14b: Charts constructed using biodistribution data. After the 1 day timepoint, the antibody began to evidently and clearly accumulate and remain in the tumor. High initial uptake in the blood was a result of the initial injection of the radiolabeled antibodies into the bloodstream. High initial uptake in the heart and lungs was likely due to early aggregation of the antibodies in said areas. Consistently high uptake in the kidneys and liver occurred simply because the kidneys are excretory organs, and the antibodies must travel through them to exit the body, and the liver plays a role in breakdown of unnecessary chemicals (i.e., radiolabeled antibodies) in the blood.

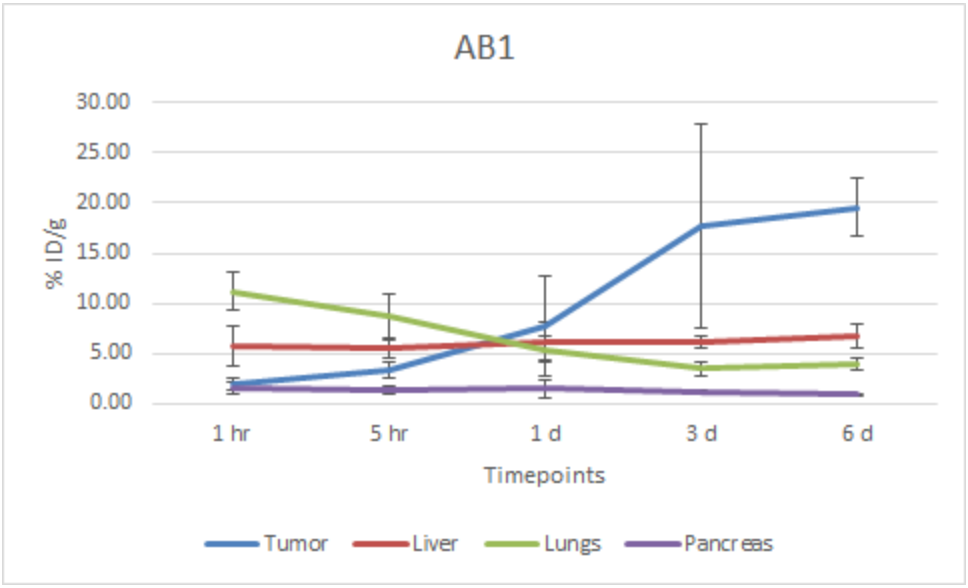

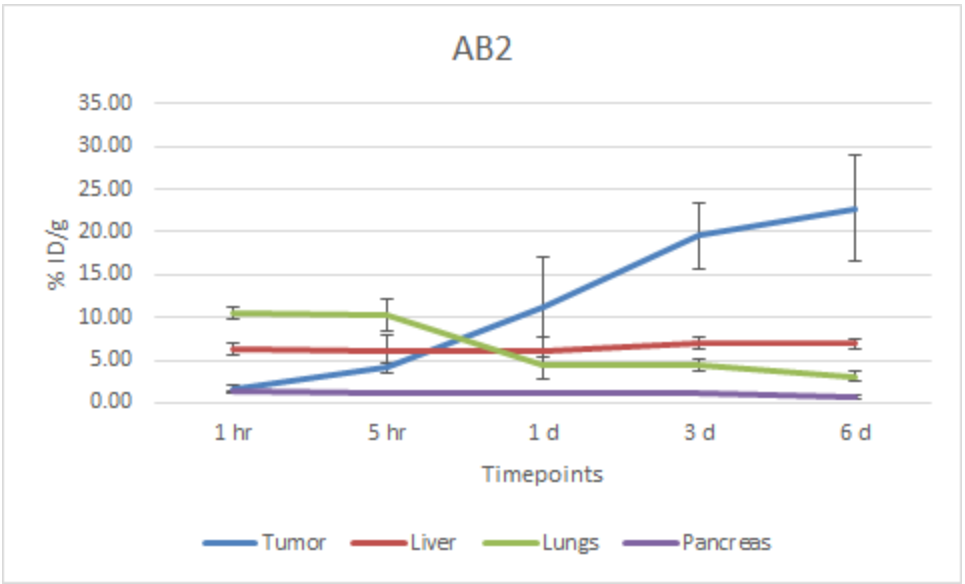

Figure 15: Additional charts constructed using biodistribution data. These show increased antibody uptake in several areas over time; in the tumor, liver, lungs, and pancreas. The tumor shows a noticeable increase over time, especially by the 1 day time point. Initial aggregation after injection is seen clearly in the lungs. Little to no uptake is shown in the pancreas itself, rather than in the PDAC tumor, showing the specificity of both AB1 and AB2. The liver also shows relatively high uptake, likely simply because the liver plays a role in breaking down materials in the body, including antibodies.

DISCUSSION:

Presented and interpreted data suggests that antibodies AB1 and AB2 bind to radiotracers [^{89}Zr]Zr-DFO-AB1 and [^{89}Zr]Zr-DFO-AB2 have high potential in detecting and delineating PDAC tumors, as shown in its high uptake in the tumor. ^{89}Zr was chosen because of its 78 hour radioactive half-life (Zhang et al., 2012), and the similar biological half-life of AB1 and AB2 (Unpublished research). Half-lives for radioisotopes and the antibodies they are binded to are usually preferred to be similar simply to allow for stable radiolabelings (Wu & Olafsen, 2011). The high uptake in almost exclusively the tumor signal that the antibodies were consistently binding to some sort of antigen found exclusively in either PDAC or malignant tissue - immunohistochemical stainings revealed that the antigen was also found in other types of malignancies, such as stomach adenocarcinoma. The high quantities naturally produced by many malignant tissues of the antigen, such as colorectal carcinoma tissue, even suggests that targeting said antigen could successfully detect other types of tumors as well, even more so than PDAC tumors. Additionally, the fact that there was minimal to no uptake of [^{89}Zr]Zr-DFO-AB1 and [^{89}Zr]Zr-DFO-AB2 essentially anywhere else, particularly in the bloodstream, suggests that the target antigen is likely not shed into circulation, at least not in large quantities. Proceeding mass spectrometry results support this conclusion (Unpublished research), revealing that the target

antigen of AB1 and AB2 was Antigen 1; Antigen 1 is anchored to the surface of cells by a glycosylphosphatidylinositol motif (Unpublished research). Although Antigen 1 was positively expressed in the salivary glands, resulting in AB1 binding to it, analysis of the immunohistochemical stainings revealed that the amount of Antigen 1 present in the salivary glands was, for the most part, substantially lower than that present in most malignant tissues, indicating that, although a bit of antibody may bind to the salivary glands, the vast majority will bind to malignant tissue. The PET images supported this, showing initial small amounts of uptake in the salivary glands, and then redistribution of the antibody throughout the body, with uptake primarily in the tumor.

CONCLUSION:

Cancer currently ranks as one of the leading causes of the death throughout the world, with a particularly prominent one being PDAC. With the establishment of a method with sufficiently high diagnosis rates, the cancer would be diagnosed more often at earlier times, resulting in fewer PDAC-related deaths. This study addresses the viable potential or monoclonal antibodies AB1 and AB2 in detecting PDAC tumors, signified by the high % ID/g of the two antibodies in the PDAC tumors of the test mice, especially between the 1 day and 6 day timepoints. The field of antibody-antigen interactions for the detection of cancerous tumors has, in the past, shown high potential for success for many different types of cancers, with many different antibody-antigen based radiotracers already being in late phases of clinical trial or even coming into clinic, such as cemiplimab and nivolumab. [^{89}Zr]Zr-DFO-AB1 and [^{89}Zr]Zr-DFO-AB2 demonstrate the potential of Antigen 1 in tumor detection of not only PDAC, but also in all other cancers that Antigen 1 is expressed in. As a result of the success from this study, one can

also argue that this showed that organoids of malignant tissues could be efficiently and reliably used to find ways of detecting and potentially even curing cancers.

BIBLIOGRAPHIES:

Abdul-Wahid, A., Cydzik, M., Fischer, N. W., Prodeus, A., Shively, J. E., Martel, A., … Gariépy, J. (2018, October 15). Serum-derived carcinoembryonic antigen (CEA) activates fibroblasts to induce a local re-modeling of the extracellular matrix that favors the engraftment of CEA-expressing tumor cells. Retrieved December 3, 2019, from https://www.ncbi.nlm.nih.gov/pmc/articles/PMC6128780/.

Attarwala, H. (2010, July). Role of antibodies in cancer targeting. Retrieved from https://www.ncbi.nlm.nih.gov/pmc/articles/PMC3217278/

Bazak, R., Houri, M., Achy, S. E., Hussein, W., & Refaat, T. (2014, November). Passive targeting of nanoparticles to cancer: A comprehensive review of the literature. Retrieved December 3, 2019, from https://www.ncbi.nlm.nih.gov/pmc/articles/PMC4179822/.

Bray, F., Ferlay, J., Soerjomataram, I., Siegel, R. L., Torre, L. A., & Jemal, A. (2018, November). Global cancer statistics 2018: GLOBOCAN estimates of incidence and mortality worldwide for 36 cancers in 185 countries. Retrieved December 3, 2019, from https://www.ncbi.nlm.nih.gov/pubmed/30207593.

Buchs, N. C., Chilcott, M., Poletti, P.-A., Buhler, L. H., & Morel, P. (2010, February 21). Vascular invasion in pancreatic cancer: Imaging modalities, preoperative diagnosis and surgical management. Retrieved December 3, 2019, from https://www.ncbi.nlm.nih.gov/pmc/articles/PMC2825328/.

Cheng, X., Zhao, G., & Zhao, Y. (2018, March 7). Combination Immunotherapy Approaches for Pancreatic Cancer Treatment. Retrieved December 3, 2019, from https://www.ncbi.nlm.nih.gov/pmc/articles/PMC5863289/.

Deshwar, A. B., Sugar, E., Torto, D., De Jesus-Acosta, A., Weiss, M. J., Wolfgang, C. L., … Yarchoan, M. (2018). Diagnostic intervals and pancreatic ductal adenocarcinoma (PDAC) resectability: a single-center retrospective analysis. Retrieved December 3, 2019, from https://www.ncbi.nlm.nih.gov/pmc/articles/PMC5909699/.

Distler, M., Rückert, F., Hunger, M., Kersting, S., & Grützmann, R. (2013, April 22). Evaluation of survival in patients after pancreatic head resection for ductal adenocarcinoma. Retrieved December 3, 2019, from https://bmcsurg.biomedcentral.com/articles/10.1186/1471-2482-13-12.

Ferreira, R. M. M., Sancho, R., Messal, H. A., Nye, E., Spencer-Dene, B., Stone, R. K., … Behrens, A. (2017, October 24). Duct- and Acinar-Derived Pancreatic Ductal Adenocarcinomas Show Distinct Tumor Progression and Marker Expression. Retrieved December 3, 2019, from https://www.ncbi.nlm.nih.gov/pmc/articles/PMC5668631/.

Garrido-Laguna, I., & Hidalgo, M. (2015, June). Pancreatic cancer: from state-of-the-art treatments to promising novel therapies. Retrieved December 3, 2019, from https://www.ncbi.nlm.nih.gov/pubmed/25824606.

Goldenberg, D. M. (1993, March). Monoclonal antibodies in cancer detection and therapy. Retrieved December 3, 2019, from https://www.ncbi.nlm.nih.gov/pubmed/8452154.

Haglund, C., Kuusela, P., & Roberts, P. J. (1989). Tumour markers in pancreatic cancer. Retrieved December 3, 2019, from https://www.ncbi.nlm.nih.gov/pubmed/2667448.

Hall, B. R., Cannon, A., Atri, P., Wichman, C. S., Smith, L. M., Ganti, A. K., … Batra, S. K. (2018, April 10). Advanced pancreatic cancer: a meta-analysis of clinical trials over thirty years. Retrieved December 3, 2019, from https://www.ncbi.nlm.nih.gov/pmc/articles/PMC5922405/.

Holloway, E. M., Capeling, M. M., & Spence, J. R. (2019, April 16). Biologically inspired approaches to enhance human organoid complexity. Retrieved December 3, 2019, from https://www.ncbi.nlm.nih.gov/pubmed/30992275.

Houghton, J. L., Zeglis, B. M., Abdel-Atti, D., Aggeler, R., Sawada, R., Agnew, B. J., … Lewis, J. S. (2015, December 29). Site-specifically labeled CA19.9-targeted immunoconjugates for the PET, NIRF, and multimodal PET/NIRF imaging of pancreatic cancer. Retrieved December 3, 2019, from https://www.pnas.org/content/112/52/15850.

Houghton, J. L., Abdel-Atti, D., Scholz, W. W., & Lewis, J. S. (2017, March 6). Preloading with Unlabeled CA19.9 Targeted Human Monoclonal Antibody Leads to Improved PET

Imaging with 89Zr-5B1. Retrieved December 3, 2019, from https://www.ncbi.nlm.nih.gov/pubmed/28191976.

Ilic, M., & Ilic, I. (2016, November 28). Epidemiology of pancreatic cancer. Retrieved December 3, 2019, from https://www.ncbi.nlm.nih.gov/pmc/articles/PMC5124974/.

Kaushik, A., Jaimini, A., Tripathi, M., D'Souza, M., Sharma, R., Mondal, A., … Dwarakanath, B. S. (2015, December). Estimation of radiation dose to patients from (18) FDG whole body PET/CT investigations using dynamic PET scan protocol. Retrieved December 3, 2019, from https://www.ncbi.nlm.nih.gov/pmc/articles/PMC4774069/.

Kenner, B. J., Go, V. L. W., Chari, S. T., Goldberg, A. E., & Rothschild, L. J. (2017). Early Detection of Pancreatic Cancer: The Role of Industry in the Development of Biomarkers. Retrieved December 3, 2019, from https://www.ncbi.nlm.nih.gov/pmc/articles/PMC5647107/.

Khan, F. H. (2013, November 15). Antibodies and Their Applications. Retrieved December 3, 2019, from https://www.sciencedirect.com/science/article/pii/B9780124160026000250.

Little, J. B. (1970, January 1). Principal Cellular and Tissue Effects of Radiation. Retrieved December 3, 2019, from https://www.ncbi.nlm.nih.gov/books/NBK12344/.

Ljubimova, J. Y., & Holler, E. (2012, October). Biocompatible nanopolymers: the next generation of breast cancer treatment? Retrieved December 3, 2019, from https://www.ncbi.nlm.nih.gov/pmc/articles/PMC4086916/.

Lukovac, S. (1970, January 1). Intestinal Crypt Organoids as Experimental Models. Retrieved December 3, 2019, from https://www.ncbi.nlm.nih.gov/books/NBK500164/.

Mukherjee, B., Satapathy, B. S., Mondal, L., Dey, N. S., & Maji, R. (2013). Potentials and challenges of active targeting at the tumor cells by engineered polymeric nanoparticles. Retrieved December 3, 2019, from https://www.ncbi.nlm.nih.gov/pubmed/24910012.

National Research Council (US) Committee on Methods of Producing MonoclonalAntibodies. (1999, January 1). Generation of Hybridomas: Permanent Cell Lines Secreting Monoclonal Antibodies. Retrieved December 3, 2019, from https://www.ncbi.nlm.nih.gov/books/NBK100203/.

Olafsen, T., & Wu, A. M. (2010, May). Antibody vectors for imaging. Retrieved December 3, 2019, from https://www.ncbi.nlm.nih.gov/pmc/articles/PMC2853948/.

Pelosi, E., Castelli, G., & Testa, U. (2017, November 18). Pancreatic Cancer: Molecular Characterization, Clonal Evolution and Cancer Stem Cells. Retrieved December 3, 2019, from https://www.ncbi.nlm.nih.gov/pmc/articles/PMC5744089/.

Poruk, K. E., Gay, D. Z., Brown, K., Mulvihill, J. D., Boucher, K. M., Scaife, C. L., … Mulvihill, S. J. (2013, March). The clinical utility of CA 19-9 in pancreatic adenocarcinoma: diagnostic and prognostic updates. Retrieved December 3, 2019, from https://www.ncbi.nlm.nih.gov/pmc/articles/PMC4419808/.

Safi, F., Roscher, R., & Beger, H. G. (1989, December). Tumor markers in pancreatic cancer. Sensitivity and specificity of CA 19-9. Retrieved December 3, 2019, from https://www.ncbi.nlm.nih.gov/pubmed/2613165.

Smigiel, J. M., Parameswaran, N., & Jackson, M. W. (2018, January 10). Targeting Pancreatic Cancer Cell Plasticity: The Latest in Therapeutics. Retrieved December 3, 2019, from https://www.ncbi.nlm.nih.gov/pmc/articles/PMC5789364/.

Sunwoo, H. H., & Suresh, M. R. (2013, February 15). Cancer Markers. Retrieved December 3, 2019, from https://www.sciencedirect.com/science/article/pii/B9780080970370000671.

Swords, D. S., Mone, M. C., Zhang, C., Presson, A. P., Mulvihill, S. J., & Scaife, C. L. (2015, October). Initial Misdiagnosis of Proximal Pancreatic Adenocarcinoma Is Associated with Delay in Diagnosis and Advanced Stage at Presentation. Retrieved December 3, 2019, from https://www.ncbi.nlm.nih.gov/pubmed/26286368.

Tong, H.-X., Zhang, L., Rong, Y.-F., Wang, D.-S., Kuang, T. T., Xu, X.-F., … Jin, D. A.-Y. (2015, January). Long-term survival following total pancreatectomy and superior mesenteric-portal vein resection for pancreatic ductal adenocarcinoma: A case report. Retrieved December 3, 2019, from https://www.ncbi.nlm.nih.gov/pmc/articles/PMC4246678/.

Torchilin, V. P. (2010). Passive and active drug targeting: drug delivery to tumors as an example. Retrieved December 3, 2019, from https://www.ncbi.nlm.nih.gov/pubmed/20217525.

Verger, A. (2017, September 27). PET Imaging in Glioblastoma: Use in Clinical Practice. Retrieved December 3, 2019, from https://www.ncbi.nlm.nih.gov/books/NBK469986/.

Viola-Villegas, N. T., Rice, S. L., Carlin, S., Wu, X., Evans, M. J., Sevak, K. K., … Lewis, J. S. (2013, November). Applying PET to broaden the diagnostic utility of the clinically validated CA19.9 serum biomarker for oncology. Retrieved December 3, 2019, from https://www.ncbi.nlm.nih.gov/pmc/articles/PMC4274751/.

Xu, H., Jiao, Y., Qin, S., Zhao, W., Chu, Q., & Wu, K. (2018, December 5). Organoid technology in disease modelling, drug development, personalized treatment and regeneration medicine. Retrieved December 3, 2019, from https://www.ncbi.nlm.nih.gov/pmc/articles/PMC6282260/.

Xu, H., Lyu, X., Yi, M., Zhao, W., Song, Y., & Wu, K. (2018, September 15). Organoid technology and applications in cancer research. Retrieved December 3, 2019, from https://www.ncbi.nlm.nih.gov/pmc/articles/PMC6139148/.

Yasuda, S., Ide, M., Fujii, H., Nakahara, T., Mochizuki, Y., Takahashi, W., & Shohtsu, A. (2000, December). Application of positron emission tomography imaging to cancer screening. Retrieved December 3, 2019, from https://www.ncbi.nlm.nih.gov/pmc/articles/PMC2363454/.

Zhang, Y., Hong, H., & Cai, W. (2011, April). PET tracers based on Zirconium-89. Retrieved from https://www.ncbi.nlm.nih.gov/pmc/articles/PMC3246366/.